PERGAMON

International Journal of Multiphase Flow 26 (2000) 1981–2004

International Journal of Multiphase Flow

www.elsevier.com/locate/ijmulflow

Flow between parallel walls containing the lines of neutrally buoyant circular cylinders

Takaji Inamuro*, Koji Maeba [1], Fumimaru Ogino

Department of Chemical Engineering, Graduate School of Engineering, Kyoto University, Kyoto, 606-8501, Japan

Received 23 February 1999; received in revised form 31 December 1999

Abstract

The motions of a single and two lines of neutrally buoyant circular cylinders in fluid between flat parallel walls are numerically investigated over the range of the Reynolds number of $12 < Re < 96$, the ratio of the diameter of the cylinder D_s to the channel width D of $0.25 \leq D_s/D \leq 0.5$, and the ratio of the streamwise spacing of the cylinders L to the channel width of $0.75 \leq L/D \leq 2$. The lattice Boltzmann method is used for computations of the fluid phase and the cylinders are moved according to Newton's law of motion. The Segré–Silberberg effect is found for both a single and two lines of cylinders. It is also found that for two lines of cylinders with $D_s/D = 0.25$ and $L/D = 1$, the equilibrium positions of the two lines are arranged to be staggered with respect to each other in the flow direction. The effects of the Reynolds number Re, D_s/D, and L/D on the equilibrium position of the lines of cylinders and on the friction factor of the cylinder–fluid mixture are presented and discussed.

1. Introduction

The problem of the particle motion in shear flows is important not only in many engineering fields such as the handling of a fluid–solid mixture in a slurry, colloid, and fluidized bed, but also in biological fields in connection with blood flow in capillaries. Therefore, such problems have been investigated experimentally and theoretically by many researchers.

* Corresponding author. Tel.: +81-75-753-5581; fax: +81-75-761-7695.
E-mail address: inamuro@cheme.kyoto-u.ac.jp (T. Inamuro).
[1] Present address: Takeda Chemical Industries Ltd., Osaka, 532-0024, Japan.

0301-9322/00/$ - see front matter
PII: S0301-9322(00)00007-0

A particularly important experimental study on the motion of particles in a pipe flow was performed by Segré and Silberberg (1961). They discovered that neutrally buoyant particles in a pipe flow migrate laterally away both from the wall and the centerline and reach a certain equilibrium lateral position. Karnis et al. (1966) verified the same phenomenon and observed that particles stabilize midway between the centerline and the wall, closer to the wall for larger flow rates and closer to the center for larger particles. They deduced that these phenomena are due to an inertia effect of the flow. Tachibana (1973) found experimentally that the lateral migration of spheres in pipe flows depends mainly on the ratio of the sphere diameter to the pipe diameter and that the phenomenon is clearly observed if this ratio exceeds about 0.2.

On the theoretical side, perturbation theories have been used to understand the lateral migration. Saffman (1965) obtained the lift on a spherical particle in a shear flow in an unbounded domain. Ho and Leal (1974) and Vasseur and Cox (1976) investigated the lateral migration of a spherical particle in both a Couette flow and a plane Poiseuille flow bounded by two infinite plane walls. These theories for the bounded domain are valid for small channel Reynolds numbers. Schonberg and Hinch (1989) extended Saffman's analysis to a small sphere in a plane Poiseuille flow for the channel Reynolds number of order unity, and McLaughlin (1993) studied the lift on a small sphere in wall-bounded linear shear flows for small particle Reynolds numbers. For these theories to be valid, the dimensionless radius of the sphere must be small. In general, however, these perturbation theories can represent the motion of particles only subject to the severe restrictions that the Reynolds numbers be small and/or the particles be small, compared with the channel width.

On the other hand, numerical simulations have been used for the problem of particle motion in shear flows. Direct numerical simulations require no restrictions such as small Reynolds numbers, small particles, and so on. Thus, it is possible to compute the motion of particles not only around the center of a channel but also near a wall at various Reynolds numbers. Feng et al. (1994) investigated the motion of a circular particle in a Couette and Poiseuille flow using a finite-element method and obtained qualitative agreement with the results of perturbation theories and of experiments. Nirschl et al. (1995) carried out three-dimensional calculations of flows around a spherical particle between two moving walls using a finite-volume method with a Chimera grid scheme, but they were not concerned about the motion of the particle.

Considering particle transport in pipes and blood flow in capillary vessels (in which the red blood cells represent particles), there exists a need to investigate the motion of the lines of particles and the pressure drop in flows of a fluid–solid mixture in pipes. Wang and Skalak (1969) investigated analytically a Stokes flow through a pipe of a liquid containing spherical particles located on the axis of the pipe and equally spaced. Chen and Skalak (1970) applied the same method for a line of spheroidal particles. They obtained the interaction between particles and the pressure drop in the pipe. In their analysis, however, the lateral motion of particles is not considered and the Reynolds number is assumed to be so low that inertia terms may be neglected.

In this paper, we use the lattice Boltzmann method (McNamara and Zanetti, 1988; Higuera and Jimenez, 1989; Chen et al., 1991; Qian et al., 1992) to investigate the flow containing the lines of neutrally buoyant circular cylinders between flat-parallel walls. The lattice Boltzmann method has been used for simulating solid–fluid suspensions of spheres by Ladd (1994, 1996, 1997), cylinders by Aidun and Lu (1995), and non-spherical particles by Qi (1997, 1999) and by

Aidun et al. (1998). In particular, Ladd (1996, 1997) carried out dynamic simulations of bulk sedimentation using up to 32,000 spheres. However, the interactions between solid particles and walls and the motion of solid particles near walls have not been thoroughly examined. Here we investigate the equilibrium position of circular cylinders and examine the friction factor of a cylinder–fluid mixture flow between parallel walls at various Reynolds numbers, for various ratios of the diameter of the cylinder to the channel width, and for various ratios of the streamwise spacing of the cylinders to the channel width.

2. Numerical method

We use the lattice Boltzmann method for the computation of the fluid phase and Newton's law of motion for the computation of the motion of the lines of cylinders. At each time step the force and torque acting on each cylinder are obtained from the flow field stress tensor and then the motion of the cylinder is explicitly updated.

2.1. Lattice Boltzmann method

In the lattice Boltzmann method, a modeled gas, which is composed of identical particles whose velocities are restricted to a finite set of vectors, is considered. Hereafter, we use non-dimensional variables defined by a characteristic length H, a characteristic particle speed c, a characteristic time scale $t_0 = H/U$ where U is a characteristic flow speed, and a reference density ρ_0 (see Inamuro et al., 1997). The characteristic particle speed c is related to the internal energy e by $e = \frac{1}{3}c^2$ (Inamuro et al., 1997), and c is chosen by using this relation in the following where the internal energy is assumed to be constant. The nine-velocity model (Nadiga, 1992; Qian et al., 1992) is used in the following calculations. The model has the velocity vectors, $\boldsymbol{c}_1 = \boldsymbol{0}$, $\boldsymbol{c}_i = [\cos(\pi(i-2)/2),\ \sin(\pi(i-2)/2)]$ for $i = 2, 3, 4, 5$, and $\boldsymbol{c}_i = \sqrt{2}[\cos(\pi(i-\frac{11}{2})/2),\ \sin(\pi(i-\frac{11}{2})/2)]$ for $i = 6, 7, 8, 9$, as shown in Fig. 1. The evolution of the particle distribution function $f_i(\boldsymbol{x}, t)$ with the velocity $\boldsymbol{c}_i$ at the point $\boldsymbol{x}$ and time t is computed by the following equations:

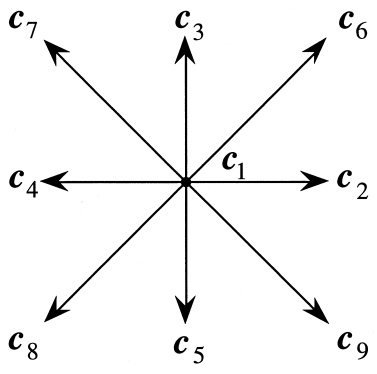

Fig. 1. The nine-velocity model.

$$f_i(\boldsymbol{x}+\boldsymbol{c}_i\Delta x,\, t+\Delta t)-f_i(\boldsymbol{x},\, t)=-\frac{1}{\tau}\left[f_i(\boldsymbol{x},\, t)-f_i^{\mathrm{eq}}(\boldsymbol{x},\, t)\right] \quad \text{for } i=1, 2, \ldots, 9, \tag{1}$$

where Δx is a lattice spacing, Δt is a time step, f_i^{eq} is an equilibrium distribution function, and τ is a single relaxation time. It is noted that Δt is chosen so that the particles travel one lattice spacing during the time step. A suitable equilibrium distribution function of the model is given by Qian et al. (1992)

$$f_i^{\mathrm{eq}}=E_i\rho\left[1+3\boldsymbol{c}_i\cdot\boldsymbol{u}+\frac{9}{2}(\boldsymbol{c}_i\cdot\boldsymbol{u})^2-\frac{3}{2}\boldsymbol{u}\cdot\boldsymbol{u}\right], \tag{2}$$

where $E_1=4/9$, $E_2=E_3=E_4=E_5=1/9$, and $E_6=E_7=E_8=E_9=1/36$. The fluid density ρ and the fluid velocity $\boldsymbol{u}$ are calculated in terms of the particle distribution function by

$$\rho=\sum_{i=1}^{9} f_i, \tag{3}$$

$$\boldsymbol{u}=\frac{1}{\rho}\sum_{i=1}^{9} f_i\boldsymbol{c}_i, \tag{4}$$

and the pressure p is related to the density ρ by

$$p=\frac{1}{3}\rho. \tag{5}$$

We can also calculate the stress tensor $\boldsymbol{\sigma}=\{\sigma_{\alpha\beta}\}$ ($\alpha, \beta = x, y$) as follows (see Appendix A):

$$\sigma_{\alpha\beta}=-\frac{1}{2\tau}p\,\delta_{\alpha\beta}-\frac{\tau-\frac{1}{2}}{\tau}\sum_{i=1}^{9} f_i(c_{i\alpha}-u_\alpha)(c_{i\beta}-u_\beta), \tag{6}$$

where $\delta_{\alpha\beta}$ is the Kronecker delta. The kinematic viscosity ν is given by

$$\nu=\frac{1}{3}\left(\tau-\frac{1}{2}\right)\Delta x. \tag{7}$$

The dimensional forms of the above-mentioned variables are as follows: $c\boldsymbol{c}_i$ is the particle velocity, $H\boldsymbol{x}$ is the coordinates, $t_0 t$ is the time, $\rho_0 f_i$ is the particle distribution function, $\rho_0\rho$ is the density, $c\boldsymbol{u}$ is the fluid velocity, $\rho_0 c^2 p$ is the pressure, $\rho_0 c^2\boldsymbol{\sigma}$ is the stress tensor, and $cH\nu$ is the kinematic viscosity.

It was found by Inamuro et al. (1997) that using Eqs. (1)–(5) we can obtain the flow velocities and the pressure gradient for incompressible flow with relative errors of $O(\varepsilon'^2)$ where ε' is a modified Knudsen number which is of the same order as the lattice spacing Δx and is related to the relaxation time τ. That is, when Δx, τ, and the Reynolds number are given, the errors are proportional to the square of the Mach number U/c. In other words, the lattice Boltzmann method has compressibility intrinsically, and the errors are caused by the compressibility effect. It is also noted that the pressure gradient should be of the same order as

$(U/c)^2$ in order to ensure incompressible flow (Inamuro et al., 1997). Otherwise, we have high Mach numbers, and the compressibility effect becomes large. In a preliminary calculation of plane Poiseuille flow with a large pressure drop (Mach number is 0.3), we have an error of about 15% compared with the exact solution of incompressible flow.

The domain of computation is divided into a square lattice grid, and the cylinders are embedded in the grid. The boundary nodes representing the cylinder are made up of lattice grids surrounding the cylinder as shown in Fig. 2. The no-slip boundary condition (see Appendix B), which is based on the diffuse reflection in the kinetic theory of gases, is applied at the boundary nodes. In this condition, the particle leaving a wall is assumed to have an equilibrium distribution function with a counter slip velocity in order to cancel a slip velocity near the wall which is induced by the bounce-back boundary condition. By forcing the assumption only on leaving particles and by taking the counter slip velocity into account, we can treat a non-equilibrium state of no-slip condition at walls. The accuracy of the condition for fundamental problems is illustrated in Inamuro et al. (1995), and the accuracy for the present problem is given in Section 2.4. At each computation step the cylinder moves across the fixed grid and thus the boundary nodes representing the cylinder are changed with time.

2.2. Motion of cylinder

Let D_s and ρ_s be the diameter and the density of the cylinder, respectively. The translational velocity $\boldsymbol{u}_s$ and the angular velocity Ω of the cylinder with the mass $M = \rho_s(\pi D_s^2/4)$ and the moment of inertia $I = M(D_s^2/8)$ are described by Newton's law as follows:

$$M\frac{\mathrm{d}\boldsymbol{u}_s}{\mathrm{d}t} = \boldsymbol{F}, \tag{8}$$

$$I\frac{\mathrm{d}\Omega}{\mathrm{d}t} = T, \tag{9}$$

where $\boldsymbol{F}$ and T are the force and the torque acting on the cylinder, respectively. In previous lattice Boltzmann methods (Ladd, 1994; Aidun and Lu, 1995; Qi, 1997, 1999; Aidun et al.,

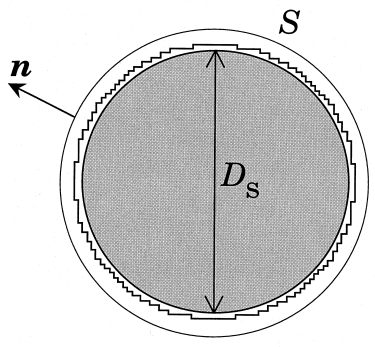

Fig. 2. A closed surface S around a cylinder with a diameter D_s and the unit outward normal vector $\boldsymbol{n}$ on S. A block of lattice grids surrounding the cylinder represents boundary nodes used in computations.

1998), the force and the torque are usually calculated by applying modified bounce-back conditions to the particle distribution functions. These conditions are somewhat heuristic, although they work well. From a hydrodynamic point of view, it is straightforward to use the stress tensor for calculating the force and the torque. Here the force and the torque acting on the cylinder are calculated from the stress tensor given by Eq. (6). However, the calculated results of the stress tensor on the cylinder are not smooth, since the circular surface is represented by the square lattice grids. Thus, we use a closed surface S which is apart from the cylinder as shown in Fig. 2 and calculate the force and torque by integrating stress tensor and momentum flux on that surface using the following equations:

$$\boldsymbol{F} = \int_S \left\{ \boldsymbol{\sigma} \cdot \boldsymbol{n} - \rho \boldsymbol{u} \left[(\boldsymbol{u} - \boldsymbol{u}_s) \cdot \boldsymbol{n} \right] \right\} \mathrm{d}S, \tag{10}$$

$$T = \int_S \boldsymbol{r} \times \left\{ \boldsymbol{\sigma} \cdot \boldsymbol{n} - \rho \boldsymbol{u} \left[(\boldsymbol{u} - \boldsymbol{u}_s) \cdot \boldsymbol{n} \right] \right\} \mathrm{d}S, \tag{11}$$

where $\boldsymbol{n}$ is the unit outward normal vector on S and $\boldsymbol{r}$ is a vector from the center of the cylinder to the point on S. In the above equations, an unsteady term is neglected because it is found in preliminary calculations that the unsteady term is negligibly small. The integral in Eqs. (10) and (11) is approximated by the quadrature of 400 points. The ρ, $\boldsymbol{u}$, and $\boldsymbol{\sigma}$ on S are calculated from the linearly interpolated values of f_i at the point on S. To determine the diameter of S, we calculated the force and torque by changing the value of the diameter of S and found that by using the values between 1.16 and $1.32D_s$ for the diameter of S we obtain almost the same force and torque. Hence, we choose the diameter of S to be $1.16D_s$ in the following calculations. The first-order Euler method with the same time step as Eq. (1) is used for the computations of Eqs. (8) and (9).

2.3. Conditions of computation

A single line of neutrally buoyant cylinders in fluid between parallel walls is considered (see Fig. 3). The distance between the two walls is D, and the inlet and outlet of the channel are a length of L apart. The density of the cylinder is equal to that of the fluid ($\rho_s = \rho$). The periodic boundary condition with a constant pressure difference Δp (see Appendix B) is used at the inlet and outlet of the channel. At $t = 0$, fluid velocity is set to be zero and the cylinders are located at $x = 0$ and L with zero velocity. In the following calculations, we define the Reynolds number Re and the friction factor f as follows:

$$Re = \frac{\bar{u}D}{\nu}, \tag{12}$$

$$f = \frac{1}{2}\frac{D}{L}\frac{\Delta p}{\frac{1}{2}\bar{\rho}\bar{u}^2}, \tag{13}$$

where $\bar{u}$ and $\bar{\rho}$ (= 1) are the time- and space-averaged velocity and density of the cylinder–fluid mixture at the inlet, respectively, after the cylinder reaches an equilibrium position. In the

present calculations, when Δx, τ, and Δp are given, $\bar{u}$ is obtained by the calculations. The Reynolds number is changed as follows. First, we choose Δx and a tentative $\bar{u}$ (A small $\bar{u}$ is desirable, since errors are proportional to $\bar{u}^2$. We choose $\bar{u} \approx 0.04$ in the following calculations.). Then, we choose τ so as to satisfy a specified Reynolds number and choose Δp so as to obtain a close value of the tentative $\bar{u}$.

2.4. Accuracy of the method

To examine the accuracy of the method, we calculated a flow over a line of circular cylinders placed at the middle of a straight channel. Aidun and Lu (1995) computed the same flow using both a finite-element method and the lattice Boltzmann method. We took the case where the cylinder is fixed and the channel walls move tangentially with a constant velocity u_w. The domain is divided into a 128×128 lattice grid and the Reynolds number is $Re = u_w D_s/\nu = 1$; these are the same conditions as used by Aidun and Lu (1995). The periodic boundary condition with zero pressure gradient is used at the inlet and outlet of the channel. We compare the results of the dimensionless force per unit area of the channel wall $f_w = F_w/(\rho u_w^2 L)$ (where F_w is the force acting the wall and is calculated by using Eq. (6)) and that of the cylinder surface $f_c = |\boldsymbol{F}|/(\pi \rho u_w^2 D_s)$ (where $\boldsymbol{F}$ is calculated by Eq. (10)) with the results of Aidun and Lu (1995) in Table 1. It is found that the present results agree with those of Aidun and Lu (1995) within 1.3% for $D_s = 60.8\Delta x$ which is nearly equal to $D_s = 50\Delta x$ used in the following calculations. In addition, we calculated the dimensionless forces f_w and f_c of a moving line of cylinders with the radius $60.8\Delta x$ and the velocity $u_s = u_w$ between fixed parallel

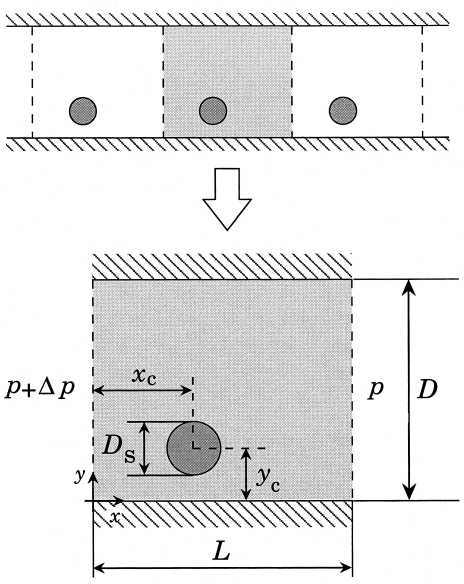

Fig. 3. The domain of computation for a single line of cylinders.The periodic boundary condition with a constant pressure difference Δp is used at the inlet and outlet of the channel.

walls. The results shown in the bottom row in Table 1 agree well with those of a fixed single line of cylinders between moving parallel walls.

3. Results and discussion

We apply the above numerical method for calculations of the flow containing either a single or two lines of neutrally buoyant circular cylinders between flat parallel walls. The dimensionless parameters of the problem are the Reynolds number Re defined by Eq. (12), the ratio of the cylinder diameter to the channel width D_s/D, and the ratio of the spacing of the cylinders to the channel width L/D which is also related to the ratio of the occupied area of the cylinder to the whole domain $\phi = \pi D_s^2/(4LD)$. To test the influence of the grid resolution, we carried out preliminary computations of a single line of the cylinders at $Re = 27.54$ for $D_s/D = 0.25$ and $L/D = 1$ using 100×100, 200×200, and 300×300 lattice grids. From these computations, it was found that the calculated results of equilibrium positions and friction factors with the 200×200 and 300×300 lattice grids agree with each other to within 0.6%. In the following computations, we use the 200×200 lattice grid for the case of $L/D = 1$. The conditions of computations and the calculated results are listed in Table 2. The computation time for case No. 1 in Table 2 required about 20 min per 10,000 time steps on a single processor of the SGI Origin 2000 workstation.

3.1. Motion of a single line of circular cylinders

First, we calculate the motion of a single line of circular cylinders with $L/D = 1$ and $D_s/D = 0.25$ at various Reynolds numbers. The lateral migration curves of the cylinders released at

Table 1
Comparison of the results by the present method with those by Aidun and Lu (1995) for the problem of a flow over a line of circular cylinders with a diameter D_s in a moving straight channel with a constant velocity u_w. The domain is divided into 128×128 lattice grids. FEM and LBM are the results with a finite-element method and with a lattice Boltzmann method by Aidun and Lu (1995), respectively. f_w and f_c are the dimensionless force per unit area of the channel wall and that of the cylinder surface, respectively. Error is evaluated based on the result by FEM

Case	Method	τ	$u_w(u_s)$	f_c	Error (%)	f_w	Error (%)
I	FEM	–	−0.04	0.966	–	0.137	–
($D_s = 10.8\Delta x$)	LBM	1.796	−0.04	1.022	5.8	0.132	−3.6
	Present	1.796	−0.04	1.053	9.0	0.142	3.6
II	FEM	–	−0.02	1.158	–	0.316	–
($D_s = 20.8\Delta x$)	LBM	1.748	−0.02	1.229	6.1	0.313	−0.9
	Present	1.748	−0.02	1.251	8.0	0.322	1.9
III	FEM	–	−0.01	2.067	–	1.543	–
($D_s = 60.8\Delta x$)	LBM	2.324	−0.01	2.054	−0.6	1.532	−0.7
	Present	2.324	−0.01	2.093	1.3	1.561	1.2
	Present[a]	2.324	(0.01)	2.094		1.562	

[a] The results of a moving line of circular cylinders with the velocity u_s between fixed parallel walls.

Table 2
The conditions of each computation and the calculated results. Nos. 1–14 are lists for a single line of cylinders and Nos. 15–19 are for two lines of cylinders. For the single line, the Reynolds number Re, the ratio of the cylinder diameter to the channel width D_s/D, and the ratio of the occupied area of the cylinder to the whole domain $\phi = \pi D_s^2/(4LD)$ are changed in Nos. 1–6, in Nos. 7–11, and in Nos. 12–14, respectively. For the two lines, only the Reynolds number is changed in Nos. 15–19. For $u_s/\bar{u}$, $D_s\Omega/2\bar{u}$, and y_c in Nos. 15–19, upper and lower numbers correspond to cylinders B and A, respectively, in Fig. 16

No.	τ	Δp	$D/\Delta x$	$L/\Delta x$	D_s/D	ϕ	$\bar{u}$	$u_s/\bar{u}$	$D_s\Omega/2\bar{u}$	Re	y_c	$f/(12/Re)$
1	2.45	1.763×10^{-3}	200	200	0.25	0.04909	0.04137	1.129	−0.1652	12.73	0.2745	1.093
2	1.4	8.167×10^{-4}	200	200	0.25	0.04909	0.04131	1.123	−0.1655	27.54	0.2733	1.098
3	1.07	5.133×10^{-4}	200	200	0.25	0.04909	0.04091	1.120	−0.1643	43.07	0.2728	1.101
4	0.95	4.100×10^{-4}	200	200	0.25	0.04909	0.04118	1.119	−0.1632	54.91	0.2723	1.103
5	0.86	3.270×10^{-4}	200	200	0.25	0.04909	0.04110	1.118	−0.1615	68.50	0.2716	1.105
6	0.757	2.337×10^{-4}	200	200	0.25	0.04909	0.04101	1.119	−0.1573	95.74	0.2706	1.108
7	1.4	6.133×10^{-4}	200	150	0.25	0.06545	0.04010	1.103	−0.1708	26.73	0.2645	1.133
8	1.4	7.167×10^{-4}	200	171	0.25	0.05741	0.04164	1.115	−0.1675	27.76	0.2697	1.116
9	1.4	9.800×10^{-4}	200	240	0.25	0.04091	0.04131	1.123	−0.1621	27.96	0.2750	1.082
10	1.4	1.223×10^{-3}	200	300	0.25	0.03273	0.04255	1.138	−0.1590	28.37	0.2799	1.065
11	1.4	1.633×10^{-3}	200	400	0.25	0.02454	0.04325	1.154	−0.1557	28.83	0.2850	1.049
12	1.252	1.167×10^{-3}	167	239	0.30	0.04919	0.04123	1.133	−0.1788	27.47	0.2875	1.099
13	1.063	2.087×10^{-3}	125	320	0.40	0.04909	0.04146	1.178	−0.1855	27.64	0.3280	1.092
14	0.95	3.207×10^{-3}	100	400	0.50	0.04909	0.04135	1.225	−0.1554	27.57	0.3798	1.077
15	2.3	1.790×10^{-3}	200	200	0.25	0.09817	0.04259	1.112	−0.1675	14.20	0.2734	1.168
								1.109	0.1675		0.7267	
16	1.4	8.967×10^{-4}	200	200	0.25	0.09817	0.04234	1.103	−0.1672	28.23	0.2715	1.176
								1.104	0.1674		0.7285	
17	1.1	5.967×10^{-4}	200	200	0.25	0.09817	0.04222	1.101	−0.1660	42.22	0.2709	1.190
								1.101	0.1662		0.7292	
18	0.86	3.600×10^{-4}	200	200	0.25	0.09817	0.04205	1.101	−0.1621	70.08	0.2700	1.186
								1.101	0.1622		0.7299	
19	0.74	2.180×10^{-4}	200	200	0.25	0.09817	0.03819	1.104	−0.1580	95.47	0.2700	1.189
								1.104	0.1581		0.7299	

different initial positions between the centerline and the lower wall are shown in Fig. 4. It is found from Fig. 4 that in spite of the initial positions, the cylinder migrates to the same equilibrium position at $y_c/D = 0.2733$, which is a little closer to the centerline than the midpoint between the centerline and the lower wall. That is, the Segré–Silberberg effect is found even for a line of circular cylinders between parallel walls. Fig. 5 shows the profiles of the fluid velocity in the x-direction u_x at the relative positions $(x - x_c)/L = 0$, 1/4, 1/2, and 3/4 (x_c: the x position of the center of the cylinder) after the cylinder reaches the equilibrium position. At $(x - x_c)/L = 1/2$ the profile is almost equal to a parabolic curve. At $(x - x_c)/L = 1/4$ and 3/4, both the profiles almost coincide and are retarded by the influence of the cylinder. At $x = x_c$, the velocity is maximum near the centerline, and the profile in the region between the cylinder and the lower wall has a different feature from those at the other positions, presenting an upward convex curve. The pressure field in the domain is shown in Fig. 6. The pressure field is similar to that of a circular particle in a Poiseuille flow calculated by Feng et

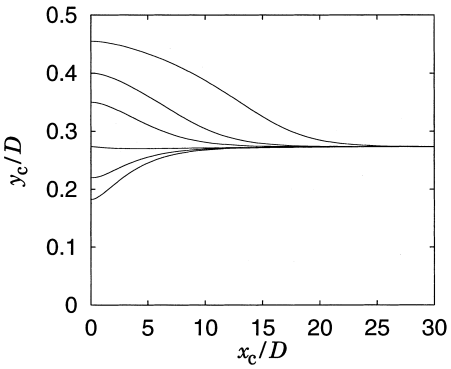

Fig. 4. Lateral migrations from different initial positions of a single line of cylinders at $Re = 27.54$ with $D_s/D = 0.25$ and $\phi = 0.04909$.

al. (1994). It is seen that a high pressure region appears on the front lower surface and on the rear upper surface of the cylinder, and a low pressure region appears on the rear lower surface of the cylinder. It is noted that an opposite pressure gradient exists between the cylinder and the lower wall. The opposite pressure gradient causes the velocity profile between the cylinder and the lower wall at $x = x_c$ to be different from those at other positions as explained in Fig. 5. Fig. 7 shows lateral migration curves of the cylinder from the same initial position at the different Reynolds numbers $Re = 12.73$, 27.54, and 95.74. It is seen that the cylinder migrates faster and reaches a point closer to the wall as the Reynolds number increases. Moreover, at $Re = 95.74$, the cylinder overshoots and oscillates a little before reaching the equilibrium

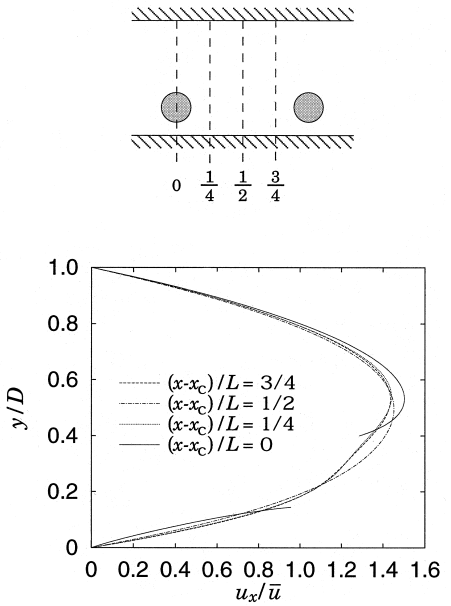

Fig. 5. Velocity profiles of a single line of cylinders at $Re = 27.54$ with $D_s/D = 0.25$ and $\phi = 0.04909$.

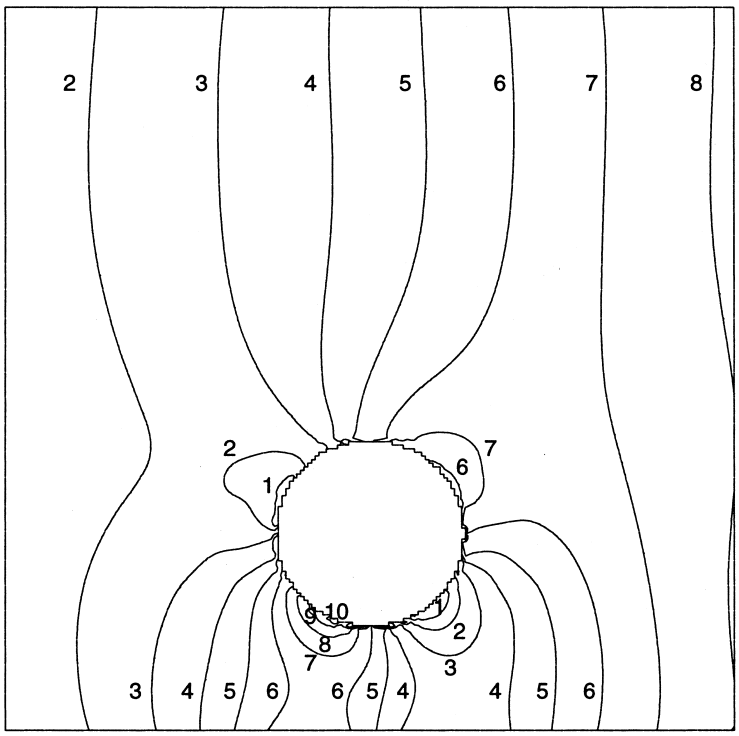

No.	p^*
1	0.8714
2	0.7437
3	0.6159
4	0.4881
5	0.3603
6	0.2325
7	0.1048
8	-0.0230
9	-0.1507
10	-0.2785

Fig. 6. Pressure distribution contours of a single line of cylinders at $Re = 27.54$ with $D_s/D = 0.25$ and $\phi = 0.04909$. $p^* = (p - \bar{p}_{(x-x_c)/L=1/2})/\frac{1}{2}\bar{\rho}\,\bar{u}^2$ where $\bar{p}_{(x-x_c)/L=1/2}$ is the space-averaged pressure at $(x - x_c)/L = 1/2$.

position, while at the lower Reynolds numbers the cylinder approaches the equilibrium position monotonically. The equilibrium positions y_s/D at various Reynolds numbers are shown in Fig. 8. The equilibrium position moves to the wall as the Reynolds number increases. The same feature of the equilibrium position against the Reynolds number is also found in the computation of a cylinder between parallel walls by Feng et al. (1994) and in the experiment of

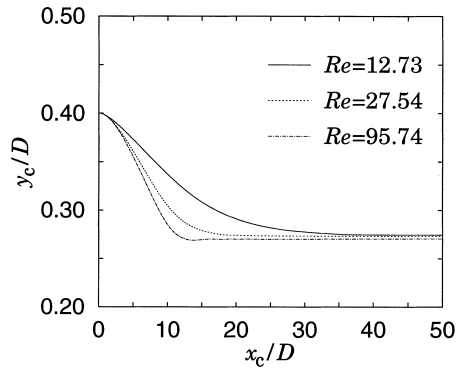

Fig. 7. Lateral migrations of a single line of cylinders at different Reynolds numbers.

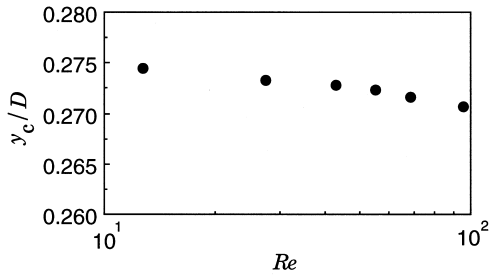

Fig. 8. Equilibrium position of the center of the cylinder y_c versus Reynolds number Re for a single line of cylinders with $D_s/D = 0.25$ and $\phi = 0.04909$.

sphere particles in a pipe flow by Karnis et al. (1966). We calculate the friction factor using Eq. (13) after the cylinder reaches the equilibrium position. The ratio of the calculated friction factor to that of flow without cylinders ($= 12/Re$) is shown against various Reynolds numbers in Fig. 9. The fact that the ratios are larger than unity is caused by a pressure excess needed to carry the cylinder. It is found from Fig. 9 that the ratio of the friction factor increases slightly as the Reynolds number increases. Fig. 10 shows the shear stress on the parallel walls. In the figure the shear stress is normalized by that of the Poiseuille flow without cylinders at the same Reynolds number. It is seen that on the lower wall the shear stress is smaller than that of the Poiseuille flow in the region under the cylinder, becomes larger in the region near the edge of the cylinder, and decreases in the region far away from the cylinder. In contrast, on the upper wall the shear stress is larger than that of the Poiseuille flow in the region near the cylinder and reaches that of the Poiseuille flow in the region far away from the cylinder. Also, the shear stress at $Re = 95.74$ becomes larger than that at $Re = 12.73$ on both the upper and lower walls, and this corresponds to the results described in Fig. 9. Another interesting feature is that the difference of the shear stress between $Re = 95.74$ and 12.73 becomes much larger on the lower wall behind the cylinder probably due to the change of the wake behind the cylinder caused by inertia effect. Thus, it is considered that the increase in the friction factor with the Reynolds number arises mainly from the inertia effect of the flow.

Next, we calculate the motion of a single line of cylinders with $D_s/D = 0.25$ at $Re \approx 27$ with various values of the spacing of the cylinders L/D. As L/D is changed, the ratio of the area

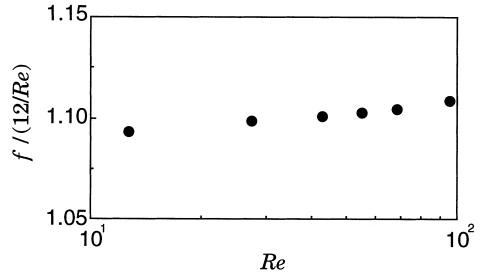

Fig. 9. The ratio of the friction factor f to that of flow without cylinders ($= 12/Re$) versus Reynolds number Re for a single line of cylinders with $D_s/D = 0.25$ and $\phi = 0.04909$.

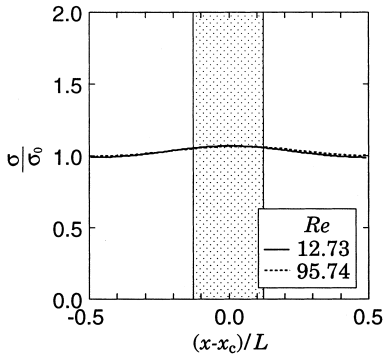

(a)

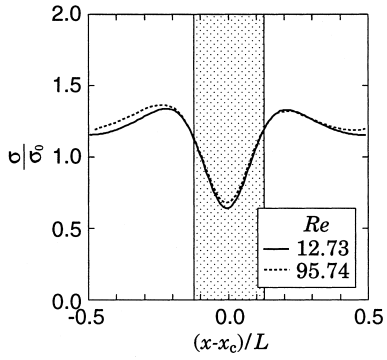

(b)

Fig. 10. Shear stresses σ on parallel walls for a single line of cylinders for different Reynolds numbers with $D_s/D = 0.25$ and $\phi = 0.04909$. The shear stress is normalized by that of the Poiseuille flow without cylinders σ_0. The shadow indicates the region where the cylinder exists. (a) On the upper wall; (b) on the lower wall.

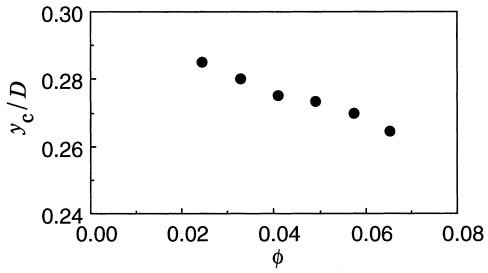

Fig. 11. Equilibrium position of the center of the cylinder y_c versus the ratio of the occupied area of the cylinder to the whole domain ϕ for a single line of cylinders with $D_s/D = 0.25$ and $Re \approx 27$.

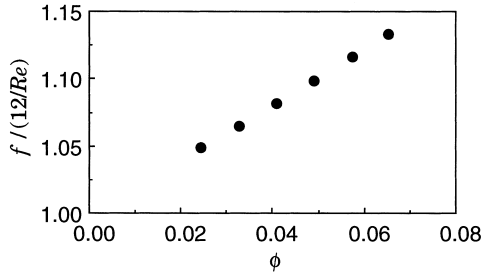

Fig. 12. The ratio of the friction factor f to that of flow without cylinders ($= 12/Re$) versus the ratio of the occupied area of the cylinder to the whole domain ϕ for a single line of cylinders with $D_s/D = 0.25$ and $Re \approx 27$.

occupied by the cylinder to the whole domain, $\phi = \pi D_s^2/(4LD)$, also changes. The other two parameters are fixed at $D_s/D = 0.25$ and $Re \approx 27$. Figs. 11 and 12 show the equilibrium position and the ratio of the friction factors against ϕ, respectively. It is found from these figures that the equilibrium position approaches the lower wall as ϕ increases and that the ratio of friction factors increases in proportion to ϕ. This linear increase of the ratio of friction factors is due to the dependence of the pressure excess on the number of cylinders in a unit length of the channel.

Finally, we investigate the effect of D_s/D at $Re \approx 27.5$ and with $\phi \approx 0.049$. Figs. 13 and 14 show the equilibrium position and the ratio of the friction factors, respectively. The equilibrium position approaches the center of the channel as the diameter of the cylinder increases. A similar experimental finding for spherical particles in a pipe flow was reported by Karnis et al. (1966). It is noted that the ratio of the friction factors becomes smaller as D_s/D increases. That is, the apparent viscosity of the cylinder–fluid mixture decreases as D_s/D increases in keeping ϕ constant, which corresponds to the Fåhræus–Lindqvist effect in blood flow (Fåhræus and Lindqvist, 1931) and the sigma phenomenon in flow of suspensions (Scott Blair, 1958). The shear stresses on the upper and lower walls for $D_s/D = 0.25$ and 0.5 are shown in Fig. 15. In the figure, the dark and light shadows indicate the regions where the cylinders of the diameter $D_s/D = 0.25$ and 0.5 exist, respectively. It is noted that since ϕ is kept constant, doubling D_s/D corresponds to halving D_s/L. The effect of the cylinder on the shear stress is larger for $D_s/D = 0.5$ than for $D_s/D = 0.25$ on both walls. In addition, on the

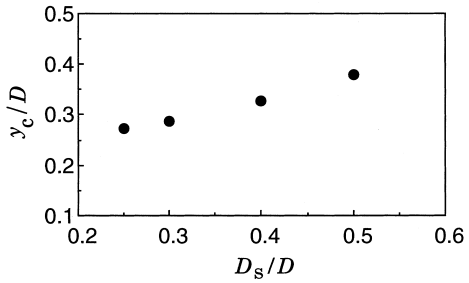

Fig. 13. Equilibrium position of the center of the cylinder y_c versus the ratio of the cylinder diameter to the channel width D_s/D for a single line of cylinders at $Re \approx 27.5$ and with $\phi \approx 0.049$.

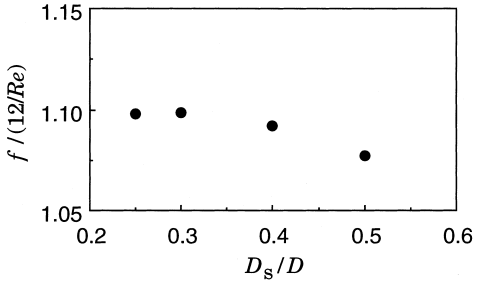

Fig. 14. The ratio of the friction factor f to that of flow without cylinders ($= 12/Re$)versus the ratio of the cylinder diameter to the channel width D_s/D for a single line of cylinders at $Re \approx 27.5$ and with $\phi \approx 0.049$.

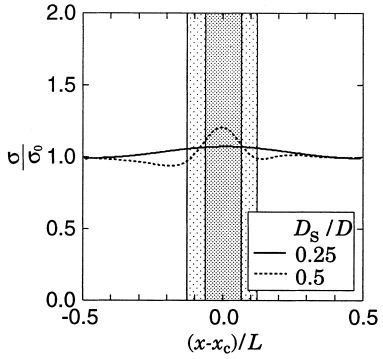

(a)

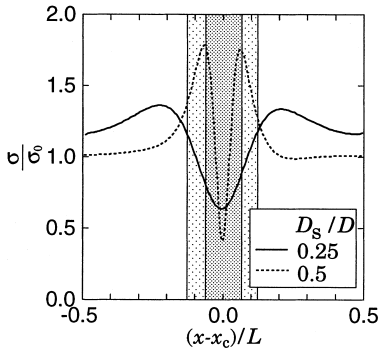

(b)

Fig. 15. Shear stresses σ on parallel walls for a single line of cylinders for different D_s/D. The shear stress is normalized by that of the Poiseuille flow without cylinders σ_0. The dark and light shadows indicate the regions where the cylinders of the diameter $D_s/D = 0.25$ and 0.5 exist, respectively. (a) On the upper wall; (b) on the lower wall.

lower wall the shear stress near the cylinder becomes larger for $D_s/D = 0.5$ than for $D_s/D = 0.25$ because of the size effect of the cylinder. Also, the shear stress in the region between the cylinders becomes smaller for $D_s/D = 0.5$ than for $D_s/D = 0.25$, since the spacing between the cylinders is smaller for $D_s/D = 0.25$ than for $D_s/D = 0.5$. Integrating the shear stress in Fig. 15, we obtain a smaller total viscous force on both the walls for $D_s/D = 0.5$ than for $D_s/D = 0.25$ as illustrated in Fig. 14. Thus, the decreasing apparent viscosity of the cylinder–fluid mixture for large D_s/D is due to the increase in the spacing between the cylinders that overcomes the size effect of the cylinder.

It is interesting to note in Table 2 that the translational velocity of the cylinder, u_s, is larger than the time- and space-averaged velocity of the cylinder–fluid mixture, $\bar{u}$, for all cases. In particular, it is clearly found that $u_s/\bar{u}$ becomes larger as D_s/D increases. The similar phenomenon has been also found in blood flow (Fåhræus, 1929).

To this point, we investigated the effects of the parameters Re, D_s/D, and ϕ over relatively small ranges. Yet there is also interest in the effects over much wider ranges of the parameters. However, there are difficulties in obtaining such solutions. For example, for $Re > 100$ we have not been able to obtain a steady solution for both the equilibrium position and the friction factor. It is possible that for high Reynolds numbers the cylinders might pass over one another and the motion of the cylinders may become much more complicated, and the restriction to a line of the equally spaced cylinders must be relaxed for that case. Further work remains in the investigation over a wide range of the parameters.

3.2. Motion of two lines of circular cylinders

Next, we calculate the motion of two lines of circular cylinders as shown in Fig. 16. A line of cylinders exists in the upper region as well as in the lower region. First, we examine the equilibrium position of the two lines of cylinders at $Re = 28.23$ and with $L/D = 1$ and $D_s/D = 0.25$. The initial positions of the upper and lower cylinders are set to be symmetrical with respect to the centerline of the channel as shown in Fig. 16. The time variations of the y positions of the cylinders A and B and the relative distance between the cylinders A and B in the x-direction are shown in Figs. 17 and 18, respectively. It is seen that in the early stage

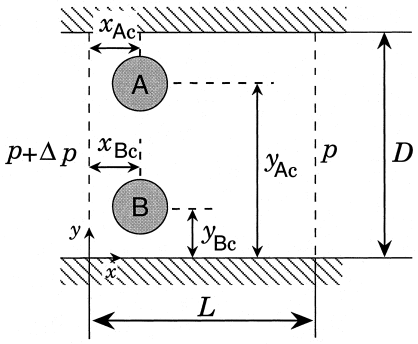

Fig. 16. The domain of computation for two lines of cylinders. The periodic boundary condition with a constant pressure difference Δp is used at the inlet and outlet of the channel.

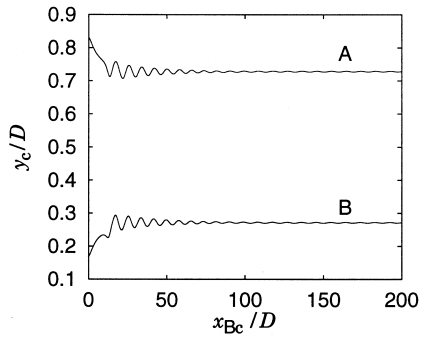

(a)

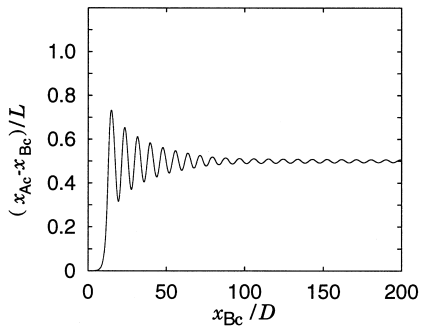

(b)

Fig. 17. Lateral migration of two lines of cylinders at $Re = 28.23$ with $D_s/D = 0.25$ and $\phi = 0.09817$. (a) The position of the center of the cylinder in y-direction; (b) the relative distance in x-direction of the cylinders A and B.

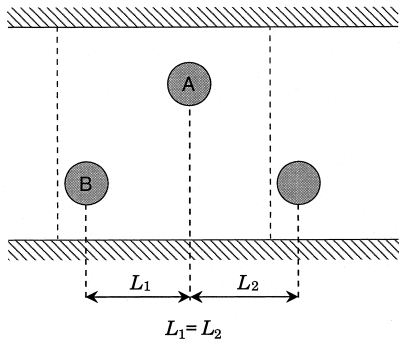

Fig. 18. Equilibrium arrangement of two lines of cylinders with $D_s/D = 0.25$ and $L/D = 1$.

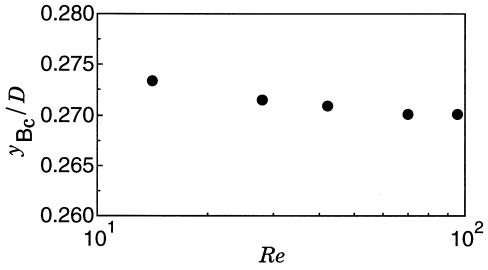

Fig. 19. Equilibrium position of the center of the cylinder B, y_{Bc}, versus Reynolds number Re for two lines of cylinders with $D_s/D = 0.25$ and $\phi = 0.09817$.

($x_{Bc}/D < 10$) the cylinders gradually migrate to the centerline, while $(x_{Ac} - x_{Bc})/L$ changes little. However, as the vertical distance between two lines becomes smaller ($x_{Bc}/D > 10$), the upper and lower cylinders begin to interact with each other and oscillate in both the x- and y-directions. Then, the oscillation decreases and the cylinders slowly reach their final equilibrium positions. In the final equilibrium state, the two lines of cylinders are found to be staggered as shown in Fig. 18. The equilibrium vertical position y_{Bc}/D of the cylinder B at various Reynolds numbers is shown in Fig. 19. As the results of there being a single line of cylinders, the equilibrium position moves toward the wall as the Reynolds number increases. Comparing these results with those of a single line of cylinders at the same Reynolds number, we can see that the cylinders migrate to almost the same vertical position in spite of another line existing in the upper region. Fig. 20 shows the calculated results for the ratio of friction factors at various Reynolds numbers. It is clear that the ratio of friction factors increases as the Reynolds number increases, which is similar to the results of a single line of cylinders. In Fig. 20 the friction factor of a single line with the same ϕ (estimated from Figs. 9 and 12) is also shown for comparison. It is seen that the friction factor of the two lines of cylinders is smaller than that of the single line of cylinders. That is, when we let the cylinder–fluid mixture move through the channel, two lines of cylinders with a staggered arrangement flow more easily than a single line of cylinders.

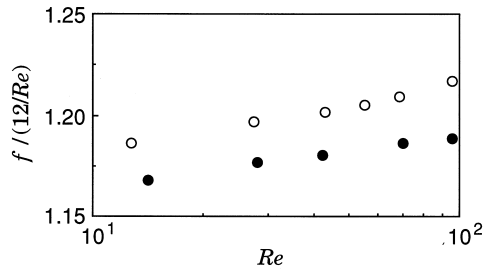

Fig. 20. The ratio of the friction factor f to that of flow without cylinders ($= 12/Re$) versus Reynolds number Re for two lines of cylinders with $D_s/D = 0.25$, and $\phi = 0.09817$. ● indicates the result of two lines of cylinders and ○ indicates the value of a single line of cylinders estimated from Figs. 9 and 12.

4. Conclusions

We have applied the lattice Boltzmann method to simulations of the flow between parallel walls containing a single and two lines of neutrally buoyant cylinders. From the computations over the parameter ranges of $12 < Re < 96$, $0.25 \leq D_s/D \leq 0.5$, and $0.75 \leq L/D \leq 2$, the following results are obtained.

1. The Segré–Silberberg effect is found to occur for both a single and two lines of cylinders.
2. For two lines of cylinders with $D_s/D = 0.25$ and $L/D = 1$ the equilibrium positions of the two lines are arranged to be staggered each other in the flow direction.
3. As the Reynolds number increases, the equilibrium cylinder position moves to the wall and the friction factor increases for both a single and two lines of cylinders.
4. As the ratio of the area occupied by the cylinder to the whole domain increases, the equilibrium cylinder position moves to the wall and the friction factor linearly increases for a single line of cylinders.
5. As the ratio of the cylinder diameter to the channel width increases, the equilibrium cylinder position moves to the centerline and the friction factor decreases for a single line of cylinders.
6. The friction factor of two lines of the cylinders is smaller than the estimated value of the friction factor of a single line of the cylinders with the same conditions.

Acknowledgements

This work was partly supported by a Grant-in-Aid (No. 10650172) for Scientific Research from the Ministry of Education, Science, Sports and Culture in Japan. The authors thank T. Suzuki for helpful discussions and Y. Onishi for assistance in preliminary computations and in drawing figures. The authors also thank Professor Daniel D. Joseph for his critical remarks and helpful suggestions on the manuscript.

Appendix A. Stress tensor

The relation between the stress tensor and the particle distribution function is obtained by using the asymptotic analysis (Inamuro et al., 1997). In that work we first put f_i in the form of series expansion of a modified Knudsen number ε' which is of the same order as the lattice spacing Δx and is related to the relaxation time τ:

$$f_i = E_i\left(1 + \varepsilon' f_i^{(1)} + \varepsilon'^2 f_i^{(2)} + \varepsilon'^3 f_i^{(3)} + \cdots\right) \quad \text{for } i = 1, 2, 3, \ldots, 9. \tag{A1}$$

Corresponding to Eq. (A1), the macroscopic variables are also expanded as follows:

$$u_\alpha = \varepsilon' u_\alpha^{(1)} + \varepsilon'^2 u_\alpha^{(2)} + \cdots, \tag{A2}$$

$$p = \frac{1}{3} + \varepsilon' p^{(1)} + \varepsilon'^{\,2} p^{(2)} + \varepsilon'^{\,3} p^{(3)} + \cdots, \tag{A3}$$

where $\alpha = x, y$. Then we obtain the fluid-dynamic type equation given by Eq. (50) of Inamuro et al. (1997) from solvability conditions. From the fluid-dynamic type equation, we obtain the stress tensor $\sigma_{\alpha\beta}$ up to $\varepsilon'^{\,3}$ as follows:

$$\begin{aligned}\sigma_{\alpha\beta} &= \sigma_{\alpha\beta}^{(0)} + \varepsilon'\sigma_{\alpha\beta}^{(1)} + \varepsilon'^{\,2}\sigma_{\alpha\beta}^{(2)} + \varepsilon'^{\,3}\sigma_{\alpha\beta}^{(3)} + O(\varepsilon'^{\,4}) \\ &= -\left(\frac{1}{3} + \varepsilon'^{\,2} p^{(2)} + \varepsilon'^{\,3} p^{(3)}\right)\delta_{\alpha\beta} + \frac{1}{3}\left(\tau - \frac{1}{2}\right)\Delta x\left[\frac{\delta}{\delta x_\alpha}\left(\varepsilon' u_\beta^{(1)} + \varepsilon'^{\,2} u_\beta^{(2)}\right)\right. \\ &\quad \left. + \frac{\delta}{\delta x_\beta}\left(\varepsilon' u_\alpha^{(1)} + \varepsilon'^{\,2} u_\alpha^{(2)}\right)\right] + O(\varepsilon'^{\,4}),\end{aligned} \tag{A4}$$

where $\delta_{\alpha\beta}$ is the Kronecker delta and $\alpha, \beta = x, y$. It is noted that $\sigma_{\alpha\beta}^{(1)} = 0$. Also, the following relation can be obtained from the asymptotic analysis:

$$\begin{aligned}&-\sum_{i=1}^{9} f_i(c_{i\alpha} - u_\alpha)(c_{i\beta} - u_\beta) \\ &= -\left(\frac{1}{3} + \varepsilon'^{\,2} p^{(2)} + \varepsilon'^{\,3} p^{(3)}\right)\delta_{\alpha\beta} + \frac{1}{3}\tau\Delta x\left[\frac{\delta}{\delta x_\alpha}\left(\varepsilon' u_\beta^{(1)} + \varepsilon'^{\,2} u_\beta^{(2)}\right) + \frac{\delta}{\delta x_\beta}\right. \\ &\quad \left.\times\left(\varepsilon' u_\alpha^{(1)} + \varepsilon'^{\,2} u_\alpha^{(2)}\right)\right] + O(\varepsilon'^{\,4}).\end{aligned}$$

From Eqs. (A4) and (A5), we can obtain

$$\sigma_{\alpha\beta} = -\frac{1}{2\tau} p\delta_{\alpha\beta} - \frac{\tau - \frac{1}{2}}{\tau}\sum_{i=1}^{9} f_i(c_{i\alpha} - u_\alpha)(c_{i\beta} - u_\beta) + O(\varepsilon'^{\,4}). \tag{A6}$$

Appendix B. Boundary conditions

B.1. No-slip boundary condition at body

We first consider the boundary condition of the cylinder–fluid interface (Inamuro et al., 1999). Let $\boldsymbol{x}_c = (x_c, y_c)$ be the position of the center of the cylinder. The boundary nodes representing the cylinder are made up of lattice grids surrounding the cylinder as shown in Fig. 2. At the boundary node $\boldsymbol{x}_w = (x_w, y_w)$, let $\boldsymbol{n}$ be the normal vector along the line connecting the node with the center of the cylinder, and $\boldsymbol{t}$ the unit tangent vector perpendicular to $\boldsymbol{n}$. The velocity vectors of the particles $\boldsymbol{c}_i$ and the velocity of the boundary node $\boldsymbol{u}_w$ are written in terms of the orthonormal basis as

$$\boldsymbol{c}_i = c_{in}\boldsymbol{n} + c_{it}\boldsymbol{t}, \tag{B1}$$

$$\boldsymbol{u}_{\mathrm{w}} = u_{\mathrm{w}n}\boldsymbol{n} + u_{\mathrm{w}t}\boldsymbol{t}, \tag{B2}$$

where $\boldsymbol{u}_{\mathrm{w}} = [u_{\mathrm{s}x} - \Omega(y_{\mathrm{w}} - y_{\mathrm{c}}),\ u_{\mathrm{s}y} + \Omega(x_{\mathrm{w}} - x_{\mathrm{c}})]$ with the translational velocity $\boldsymbol{u}_{\mathrm{s}} = (u_{\mathrm{s}x}, u_{\mathrm{s}y})$ and the angular velocity Ω of the cylinder. On the boundary node, the distribution functions with $c_{in} > 0$ are unknown. The unknown distribution functions are determined by the no-slip boundary condition (Inamuro et al., 1995). First, the unknown distribution functions are assumed to be the equilibrium distribution functions given by Eq. (2) with a counter slip velocity u_t' as follows:

$$f_i = E_i\rho'\left\{1 + 3\left[c_{in}u_{\mathrm{w}n} + c_{it}\left(u_{\mathrm{w}t} + u_t'\right)\right] + \frac{9}{2}\left[c_{in}u_{\mathrm{w}n} + c_{it}\left(u_{\mathrm{w}t} + u_t'\right)\right]^2 - \frac{3}{2}\left[u_{\mathrm{w}n}^2 + \left(u_{\mathrm{w}t} + u_t'\right)^2\right]\right\}$$
$$\text{for } c_{in} > 0, \tag{B3}$$

where ρ' and u_t' are unknown parameters. The two unknown parameters are determined on the condition that the fluid velocity on the boundary node is equal to $\boldsymbol{u}_{\mathrm{w}}$. Moreover, the fluid density at the boundary node ρ_{w} is an unknown quantity and is calculated by Eq. (3). Hence, we finally obtain three equations for the three unknowns. Assuming that $u_t'^2$ is negligibly small, we obtain the solutions

$$u_t' = \frac{\displaystyle\sum_{i(c_{in}>0)} \left[D_1(c_{in} - u_{\mathrm{w}n}) - D_2(c_{it} - u_{\mathrm{w}t})\right]A_i}{\displaystyle\sum_{i(c_{in}>0)} \left[D_2(c_{it} - u_{\mathrm{w}t}) - D_1(c_{in} - u_{\mathrm{w}n})\right]B_i}, \tag{B4}$$

$$\rho' = \frac{-\displaystyle\sum_{i(c_{in}\le 0)} (c_{in} - u_{\mathrm{w}n})f_i}{\displaystyle\sum_{i(c_{in}>0)} (c_{in} - u_{\mathrm{w}n})\left[A_i + B_i u_t'\right]}, \tag{B5}$$

$$\rho_{\mathrm{w}} = \sum_{i(c_{in}>0)} \rho'\left[A_i + B_i u_t'\right] + \sum_{i(c_{in}\le 0)} f_i, \tag{B6}$$

where

$$A_i = E_i\left[1 + 3(c_{in}u_{\mathrm{w}n} + c_{it}u_{\mathrm{w}t}) + \frac{9}{2}(c_{in}u_{\mathrm{w}n} + c_{it}u_{\mathrm{w}t})^2 - \frac{3}{2}\left(u_{\mathrm{w}n}^2 + u_{\mathrm{w}t}^2\right)\right], \tag{B7}$$

$$B_i = E_i\left[3c_{it} + 9c_{it}(c_{in}u_{\mathrm{w}n} + c_{it}u_{\mathrm{w}t}) - 3u_{\mathrm{w}t}\right], \tag{B8}$$

$$D_1 = \sum_{i(c_{in}\le 0)} (c_{it} - u_{\mathrm{w}t})f_i, \tag{B9}$$

$$D_2 = \sum_{i(c_{in} \le 0)} (c_{in} - u_{wn}) f_i. \tag{B10}$$

Substituting Eqs. (B4) and (B5) into Eq. (B3), all the unknown distribution functions on the boundary node are determined.

The same condition is used at the boundary nodes of the channel walls.

B.2. Periodic boundary condition at inlet and outlet

A periodic boundary condition with a pressure difference Δp is used on the inlet and outlet (Inamuro et al., 1999). Hereafter, the subscript 'in' and 'out' represent quantities at the inlet and outlet, respectively. At the inlet, the unknown distribution functions are f_2, f_6, and f_9. Taking account of the form of the equilibrium distribution functions given by Eq. (2) and neglecting the second- and higher-order terms of Knudsen number compared with the terms of $O(1)$, we assume that the unknown distribution functions at the inlet can be written by adding constant values C and $C/4$ to the corresponding known distribution function at the outlet:

$$f_2|_{\text{in}} = f_2|_{\text{out}} + C, \tag{B11}$$

$$f_i|_{\text{in}} = f_i|_{\text{out}} + \frac{1}{4}C \quad \text{for } i = 6, 9. \tag{B12}$$

Similarly, at the outlet the unknown distribution functions f_4, f_7, and f_8 are assumed to be written by subtracting the constant values from the corresponding known distribution function at the inlet:

$$f_4|_{\text{out}} = f_4|_{\text{in}} - C, \tag{B13}$$

$$f_i|_{\text{out}} = f_i|_{\text{in}} - \frac{1}{4}C \quad \text{for } i = 7, 8. \tag{B14}$$

Then the constant value C is determined so that the pressure difference between the inlet and outlet is equal to Δp. That is, using Eqs. (3) and (5), we get

$$C = \Delta p - \frac{1}{3}\left(f_1|_{\text{in}} - f_1|_{\text{out}} + f_3|_{\text{in}} - f_3|_{\text{out}} + f_5|_{\text{in}} - f_5|_{\text{out}}\right). \tag{B15}$$

Substituting Eq. (B15) into Eqs. (B11)–(B14), all the unknown distribution functions at the inlet and outlet are determined for the given Δp.

In addition, the unknown distribution functions at four corners of the inlet and outlet are calculated by combining the above-mentioned periodic and no-slip boundary conditions as follows. For example, at the lower corners of the inlet and outlet, we first express $f_2|_{\text{in}}$, $f_9|_{\text{in}}$, $f_4|_{\text{out}}$, and $f_8|_{\text{out}}$ by using Eqs. (B11)–(B14) with a constant value C_0. Then, applying the no-slip boundary conditions at the corners and specifying the pressure difference between the inlet and outlet, we obtain seven equations for seven unknowns. The solution for C_0 is given by

$$C_0 = \Delta p - \frac{1}{3}\left[f_1|_{\text{in}} - f_1|_{\text{out}} + 2\left(f_5|_{\text{in}} - f_5|_{\text{out}}\right)\right]. \tag{B16}$$

The solutions of other unknowns can also be obtained by using Eqs. (B4)–(B6). Thus, the unknown distribution functions are determined by Eqs. (B3) and (B11)–(B14). The same method is used at the upper corners of the inlet and outlet.

References

Aidun, C.K., Lu, Y., 1995. Lattice Boltzmann simulation of solid particles suspended in fluid. J. Stat. Phys 81, 49–61.

Aidun, C.K., Lu, Y., Ding, E., 1998. Direct analysis of particulate suspensions with inertia using the discrete Boltzmann equation. J. Fluid Mech 373, 287–311.

Chen, S., Chen, H., Martinez, D., Mathaeus, W.H., 1991. Lattice Boltzmann model for simulation of magnetohydrodynamics. Phys. Rev. Lett 67, 3776–3779.

Chen, T.C., Skalak, R., 1970. Stokes flow in a cylindrical tube containing a line of spheroidal particles. Appl. Sci. Res 22, 403–441.

Fåhræus, R., 1929. The suspension stability of the blood. Physiol. Rev 9, 241–274.

Fåhræus, R., Lindqvist, T., 1931. The viscosity of the blood in narrow capillary tubes. Amer. J. Physiol 96, 562–568.

Feng, J., Hu, H.H., Joseph, D.D., 1994. Direct simulation of initial value problems for the motion of solid bodies in a Newtonian fluid. Part 2: Couette and Poiseuille flows. J. Fluid Mech 277, 271–301.

Higuera, F., Jimenez, J., 1989. Boltzmann approach to lattice gas simulations. Europhys. Lett 9, 663–668.

Ho, B.P., Leal, L.G., 1974. Inertial migration of rigid spheres in two-dimensional unidirectional flows. J. Fluid Mech 35, 365–400.

Inamuro, T., Yoshino, M., Ogino, F., 1995. A non-slip boundary condition for lattice Boltzmann simulations (Erratum: 8, 1124). Phys. Fluids 7, 2928–2930.

Inamuro, T., Yoshino, M., Ogino, F., 1997. Accuracy of the lattice Boltzmann method for small Knudsen number with finite Reynolds number. Phys. Fluids 9, 3535–3542.

Inamuro, T., Yoshino, M., Ogino, F., 1999. Lattice Boltzmann simulation of flows in a three-dimensional porous structure. Int. J. Numer. Meth. Fluids 29, 737–748.

Karnis, A., Goldsmith, H.L., Mason, S.G., 1966. The flow of suspensions through tubes. Can. J. Chem. Engng 44, 181–193.

Ladd, A.J.C., 1994. Numerical simulations of particulate suspensions via a discretized Boltzmann equation. J. Fluid Mech. 271, 285–309, 311–339.

Ladd, A.J.C., 1996. Hydrodynamic screening in sedimenting suspensions of non-Brownian spheres. Phys. Rev. Lett 76, 1392–1395.

Ladd, A.J.C., 1997. Sedimentation of homogeneous suspensions of non-Brownian spheres. Phys. Fluids 9, 491–499.

McLaughlin, J.B., 1993. The lift on a small sphere in wall-bounded linear shear flows. J. Fluid Mech 246, 249–265.

McNamara, G., Zanetti, G., 1988. Use of the Boltzmann equation to simulate lattice-gas automata. Phys. Rev. Lett 61, 2332–2335.

Nadiga, B.T., 1992. A study of multi-speed discrete-velocity gases. Ph.D. thesis, California Institute of Technology.

Nirschl, H., Dwyer, H.A., Denk, V., 1995. Three-dimensional calculations of the simple shear flow around a single particle between two moving walls. J. Fluid Mech 283, 273–285.

Qi, D., 1997. Non-spheric colloidal suspensions in three-dimensional space. Int. J. Mod. Phys C 8, 985–997.

Qi, D., 1999. Lattice-Boltzmann simulations of particles in non-zero-Reynolds-number flows. J. Fluid Mech 385, 41–62.

Qian, Y.H., d'Humières, D., Lallemand, P., 1992. Lattice BGK models for Navier–Stokes equation. Europhys. Lett 17, 479–484.

Saffman, P.G., 1965. The lift on a small sphere in a slow shear flow. J. Fluid Mech 22, 385–400.

Schonberg, J.A., Hinch, E.J., 1989. Inertial migration of a sphere in Poiseuille flow. J. Fluid Mech 203, 517–524.
Segré, G., Silberberg, A., 1961. Radial particle displacements in Poiseuille flow of suspensions. Nature 189, 209–210.
Scott Blair, G.W., 1958. The importance of the sigma phenomenon in the study of the flow of blood. Rheol. Acta 1, 123–126.
Tachibana, M., 1973. On the behaviour of a sphere in the laminar tube flows. Rheol. Acta 12, 58–69.
Vasseur, P., Cox, R.G., 1976. The lateral migration of a spherical particle in two-dimensional shear flows. J. Fluid Mech 78, 385–413.
Wang, H., Skalak, R., 1969. Viscous flow in a cylindrical tube containing a line of spherical particles. J. Fluid Mech 38, 75–96.